

Anisotropy changes in post-menopausal osteoporosis: characterization by a new index applied to trabecular bone radiographic images

Christine Chappard · Barbara Brunet-Imbault
Gérald Lemineur · Bruno Giraudeau · Armelle Basillais
Rachid Harba · Claude-Laurent Benhamou

Received: 27 May 2004 / Accepted: 3 December 2004 / Published online: 1 February 2005
© International Osteoporosis Foundation and National Osteoporosis Foundation 2005

Abstract Bone intrinsic strength is conditioned by several factors, including material property and trabecular micro-architecture. Bone mineral density (BMD) is a good surrogate for material property. Architectural anisotropy is of special interest in mechanics-architecture relations and characterizes the degree of directional organization of a material. We have developed anisotropy indices from the Fast Fourier Transform (FFT) on bone radiographs. We have validated these indices in a cross-sectional uni-center case-control study including 39 postmenopausal women with vertebral fracture and 70 age-matched control cases. BMD was measured at the lumbar spine and femoral neck. A fractal analysis of texture was performed on calcaneus radiographs at three regions of interest (ROIs), and the result was expressed as the H parameter (fractal dimension = $H-2$). The anisotropy evaluation was based on the FFT spectrum of these three ROIs extracted on calcaneus radiographs. On the FFT spectrum, we have measured the spreading angle of the longitudinal trabeculae called the dispersion longitudinal index (DLI) and the spreading angle of the transversal trabeculae called the dispersion transversal

index (DTI). From the measured parameters, an anisotropy index was derived, and the degree of anisotropy (DA) calculated with DLI and DTI. We have compared the results from the vertebral fracture cases and control cases. The best distinction was obtained for the largest ROI located in the great tuberosity of the calcaneus for all parameters ($P < 10^{-4}$). The DA parameter showed a higher value in vertebral fracture cases (1.746 ± 0.169) than in control cases (1.548 ± 0.136); $P < 10^{-4}$, and the difference persisted after removal of the subjects with hormonal replacement therapy. The analysis of the receiver operating characteristics (ROC) has shown the best results with DA and Hmean: areas under curves (AUCs) respectively of 0.765 and 0.683, while AUCs associated to LS-BMD and FN-BMD were 0.614 and 0.591 lower, respectively. We determined the odds ratios (OR) by uni- and multivariate analysis. Crude ORs were respectively 3.91 (95% CI: 2.22–6.87) and 3.08 (95% CI: 1.72–5.52) for DA and Hmean. Crude ORs were respectively 1.71 (95% CI: 1.15–2.56) and 1.56 (95% CI: 1.05–2.31) for LS-BMD and FN-BMD. All ORs were statistically significant, and those associated to Hmean and anisotropy indices were higher than those of BMD measurements. From a multivariate analysis including anisotropy indices, Hmean, age and FN-BMD, the remaining significant ORs were respectively 6.33 (95% CI: 2.80–14.30) and 3.08 (95% CI: 1.48–6.37) for DA and Hmean. These data have shown that anisotropy indices on calcaneus radiographs can distinguish vertebral fracture cases from control cases. This analysis provides complementary information concerning the BMD and fractal parameter. These data suggest that we can improve the fracture risk evaluation by adding information related to the directional organization of trabecular bone derived from the FFT spectrum on conventional radiographic images.

C. Chappard · B. Brunet-Imbault · G. Lemineur · A. Basillais
C.-L. Benhamou (✉)
Inserm ERIT M0101, CHR Orléans, 1 rue Porte Madeleine,
45032 Orléans Cédex 1, France
E-mail: claude-laurent.benhamou@chr-orleans.fr
Tel.: +33-238744012
Fax: +33-238744024

C. Chappard · C. Benhamou
Service de Rhumatologie, Hôpital d'Orléans CHR,
1 rue Porte Madeleine, 45032 Orléans Cédex 1, France

G. Lemineur · R. Harba
3 Laboratoire Electronique Signaux Image,
Université Orléans, rue Chateauroux,
45000 Orléans, France

B. Giraudeau
4 Centre d'Investigation Clinique, Faculté de Médecine,
2bis Bd Tonnelle, 37032 Tours Cédex, France

Keywords Anisotropy · Bone mineral density · Fast Fourier transform · Micro-architecture · Osteoporosis · Radiographs · Trabecular bone

Introduction

Bone intrinsic strength is conditioned by several factors, including material properties such as bone mineral density (BMD), matrix quality and additional factors such as bone macro-architecture and trabecular micro-architecture [1]. BMD and trabecular bone micro-architecture are very important since they are part of the osteoporosis definition proposed by the World Health Organization [2]. BMD is generally used as a surrogate marker for fracture risk, while trabecular micro-architecture is not currently evaluated routinely. Connectivity and architectural anisotropy are of special interest in mechanics-architecture relations [3]. Anisotropy characterizes the degree of directional organization of a material. The more preferential direction the structure has, the more important the degree of anisotropy (DA). The anisotropy of trabecular bone depends on the skeletal site. Several bones have already been assessed for anisotropy, such as the calcaneus, hip, vertebrae and radius [4, 5, 6]. The results have shown that anisotropy is influenced by the main direction of strengths applied to the bone. For lower limbs, these forces are dependent upon gravity and walking. Gravity and muscle strength are also important for the spine. Trabecular shape and orientation are adaptive to changes in the mechanical environment, such as those induced by aging or osteoporosis [7, 8]. In these conditions some trabeculae disappear; indeed, trabeculae oriented in the direction of the main forces applied to this bone are not removed, or are removed last because of the adaptation phenomenon.

The anisotropy evaluation is possible either on three-dimensional (3D) or on two-dimensional (2D) images. The mean intercept length (MIL) method is the most currently used. The principle of this method is to fit an ellipsoid to a polar diagram plotted with the values of the MIL obtained in several directions. For each direction, the MIL is simply the total line length divided by the number of intersections between the bone-marrow interface. From the ellipsoid, the three principal MIL vector orientations and magnitudes are determined [9]. The DA can be defined as the ratio of the longest MIL vector magnitude to the smallest one. The MIL method is also used on 2D images and generates an ellipse instead of an ellipsoid. With this method the evaluation of the degree of anisotropy is generally considered as accurate [3, 10, 11]. However, some authors emphasize that the methods based on the boundary surface distribution are not fully representative of the real structure anisotropy from a stereological point of view [3, 11].

Other methods using a randomly translated point grid located on the structure have been developed, such as the volume orientation and the star volume distribution [12, 13]. An index called the Line Fraction Deviation has been developed by Geraets et al. based on the fraction of bright pixels for 180 lines rotating by steps of 15° [14]. A diagram plotting the standard

deviations of these fractions in all directions could reflect the orientation of the trabeculae.

For all of these methods the images must be previously binarized. Some methods such as fractal based texture analysis and Fast Fourier Transform (FFT) do not require previous binarization [15, 16, 17]. Jiang et al. have estimated global and directional fractal dimensions to characterize bone textural anisotropy using the Minkowski dimension [17]. In the same way, Lespessailles et al. have shown that the angular distribution of a fractal parameter derived from the maximum likelihood estimator could give information about the textural orientation [15]. From the FFT directly applied to gray level images, Wigderowitz et al. estimated variations in longitudinal and transverse trabeculae organization based on two indices called the spectral trabecular index [16]. Caligiuri et al. [18] also used the FFT to perform a structural analysis of the spine trabecular bone. The magnitude and the first moment of the power spectrum were used as predicting factors of the fracture risk, but they did not provide information about structural orientation. Cadwell et al. [19] developed a method using the Sobel filter to assign each pixel of a digitized radiograph a gradient vector. The gradient $G = (x^2 + y^2)^{1/2}$ with x and y corresponding to vertical and horizontal gradients and the direction $\Xi = \arctan(x/y)$ are calculated. The fraction-oriented edges parameter (Foe) is then evaluated using the histogram of the magnitude of the edges versus the direction of the edges. At this time, anisotropy evaluation by line fraction deviation, fractal analysis and FFT are only available on 2D images [15, 16, 17, 18, 19, 20].

We have developed and validated a texture indicator of trabecular bone radiographic images based on the fractal model of the fractional Brownian motion [21]. This fractal indicator, when applied to populations of vertebral fractures and controls, has permitted a good distinction between these populations [22, 23]. The objective of the present work was to add an anisotropy-based distinction to that offered by BMD and fractal analysis in this last population study [23]. With this aim, we have tested a new method of anisotropy evaluation and applied it to three different regions of interest (ROI) on calcaneus radiographic images. This paper describes this method and its clinical validation based on a comparison between vertebral fracture cases and control cases.

Subjects and methods

Subjects and BMD measurements

The study population already has been described elsewhere [23]. It involved a series of 99 osteoporotic fractures and 197 control women. In the present study, we have focused on vertebral fractures exclusively, thus including 39 cases. Each of these latter cases was age-matched (± 5 years), with two controls randomly

selected anytime it was possible, thus leading to the inclusion of 70 controls. The fracture cases were recruited in our rheumatology department or in the densitometry unit of this department [23]. The diagnosis of vertebral fracture was done according to Genant's criteria of vertebral deformity on lateral spine radiographs [24]. Bone mineral density (BMD) measurements of the lumbar spine (LS) and femoral neck (FN) were realized with a Hologic QDR 4500 device in all patients.

Realization of calcaneus radiographs

The procedure has been described elsewhere in detail [21]. All the radiographic processing was standardized as much as possible. All radiographic films were acquired in the same conditions: on the same X-ray clinical apparatus, with a tube voltage of 36 kV, with 18 mAs exposure conditions and Min-R film (KODAK, Paris, France). Then digitized images were obtained by scanning the radiographic films with an Agfa DuoScan scanner (AGFA GEVAERT N.V., Mortsel, Belgium). The scanning resolution was fixed at 100 μm , and all optional scanning controls were not activated (brightness, contrast, color and optical density).

Extraction of the ROI

Three different ROIs were manually extracted from the radiographic images. The first ROI called ROIa (Fig. 1) was the region usually analyzed in our fractal analysis [21]. The size of ROIa was 256 \times 256 pixels with a pixel size of 105 μm and ROI size of 27 \times 27 mm^2 . This area had a reproducible location, and mild changes did not significantly alter the reproducibility of the fractal analysis [21]. ROIa included only trabecular bone in the posterior part of the os calcis, comprising two sets of trabeculae (Fig. 1). The first set of trabeculae originated from the subtalar articular joint and diverged downwards and backwards through the waist of the calcaneus and assimilated to the longitudinal trabeculae. The second set of trabeculae started in front of the great tuberosity and swept backwards and upwards and

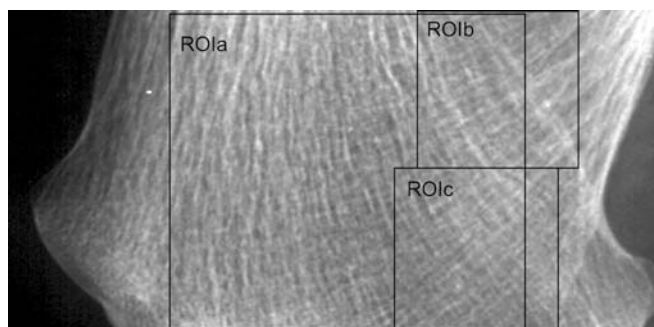


Fig. 1 Typical radiograph of calcaneus with the three ROI studied

assimilated to the transverse trabeculae [25]. The sizes of ROIb and ROIc were 128 \times 128 pixels (Fig. 1). The inferior right edge of the ROIb was positioned at the endocortical side of the inferior cortex. The ROIc was positioned below the ROIb with the right adjacent to the cortex.

Noise filtering

The low frequency noise of an image corresponds to the gray-value variations over large distances as a result of radiological artifacts and to the fat tissue projection on the radiograph. In order to remove the low frequency noise of the image to just taking account of trabecular components of the image, we applied a method described by Geraets using a Kernel box [5]. For each pixel, the average gray value of the box was allocated to the box middle pixel, and this image was called the low frequency image. The window must be small enough to extract the low frequency noise, and large enough to prevent the trabecular pattern leaking into the low frequency region. We chose a box of 25 \times 25 pixels size. The filtered image was obtained by subtracting the low-frequency image from the original image (Fig. 2).

Gray-level Fourier transform analysis

The Fourier transform represents a signal in frequency space. An image can be considered as a repartition of bright intensities in a (xOy) plan and can be expressed as a bidimensional function $f(x,y)$; the corresponding 2D Fourier transform is:

$$F(\mu, \nu) = \int_{-\infty}^{+\infty} \int_{-\infty}^{+\infty} f(x, y) e^{-2\pi i(\mu x + \nu y)} dx dy \quad (1)$$

where (μ, ν) and (x, y) are respectively the variables of the frequency and of the spatial domains.

Any periodic structure in the original spatial-domain image is represented by peaks in the frequency-domain

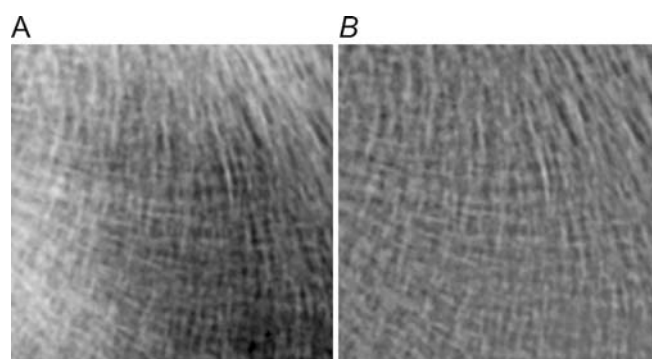


Fig. 2 Illustration of gray level images obtained before and after filtering to remove radiological artifacts and fat tissue projection. A Before filtering, B after filtering

image at a distance corresponding to the period and in direction at right angle to the original orientation. If a mild degree of disorientation is introduced in an oriented periodic structure, the frequencies of the Fast Fourier transform (FFT) spectrum are spread over an angle corresponding to the deviation of the structure in the original image (Fig. 3). By analogy, concerning trabecular bone we have hypothesized that the structure is represented by trabeculae projection, the periodicity by trabeculae projection spacing and the orientation by bone anisotropy.

The FFT was calculated on the gray level filtered images of the trabecular bone using the Visilog 5.1 software (Noesis). Then the magnitudes of the frequency images were normalized to the total magnitude of the transform to reduce the influence of the contrast in the images; the following formula was used to derive anisotropy indices.

$$\frac{|F(\mu, v)|}{\sqrt{\int_{-\infty}^{+\infty} \int_{-\infty}^{+\infty} |F(\mu, v)|^2 d\mu dv}} \quad (2)$$

Measured parameters

Inside the studied ROI, the longitudinal and transversal trabeculae could be assimilated to an oriented structure with two main directions. All the FFT spectra of the calcaneus radiographs had a cross-like shape (Fig. 4).

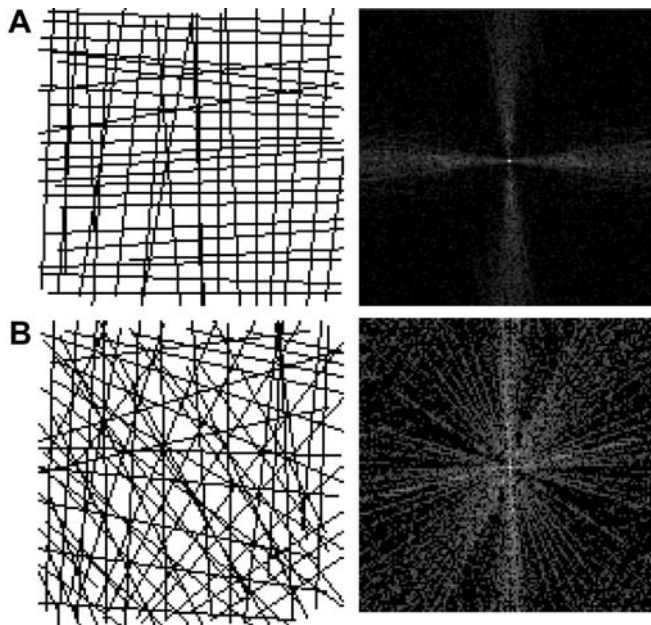


Fig. 3 **A** Synthetic image of a periodic structure aligned in two orthogonal directions. **B** Synthetic image of a structure without preferential alignment. If a degree of disorientation is introduced in an oriented periodic structure, the frequencies of the Fast Fourier transform (FFT) spectrum are spread over an angle corresponding to the deviation of the structure in the original image

The horizontal branch was indicative of the longitudinal trabeculae fabric, and the vertical branch was indicative of the transverse trabeculae fabric. In order to obtain anisotropy indices, two measures were performed on the FFT spectrum used as an image (Fig. 4). The limit between the high energy area representing trabeculae and low energy area corresponding to the noise on the FFT spectrum was visually determined by the operator. This limit was materialized by a line drawn by the operator as shown in some examples in Fig. 4. Thus, we measured manually the spreading angles of the longitudinal and the transverse trabeculae, called respectively the dispersion longitudinal index (DLI) and the dispersion transverse index (DTI). This process was performed blindly without knowledge of the diagnosis by a first skilled observer, and secondly by an unskilled observer. This last observer has worked on ROI_a.

Indices

Indices relative to the trabecular organization were derived from the measured parameters DLI and DTI and represented the disorientation of the projected trabeculae, and the degree of anisotropy (DA) was determined by the following formula:

$$DA = \frac{\pi}{DLI + DTI} \quad (3)$$

The FFT spectrum of an isotropic structure is near a disc, with a DA close to one. The more anisotropic a structure is, the more superior to one is its DA. We have illustrated typical isotropic and anisotropic structures on synthetic images (Fig. 3).

Reproducibility of measurements

In five subjects, four measurements of the right heel were performed within 1 month to assess the long-term reproducibility of the method. The results were expressed as the root mean square average coefficient of variation (RMSCV%) according to the following formula [26]:

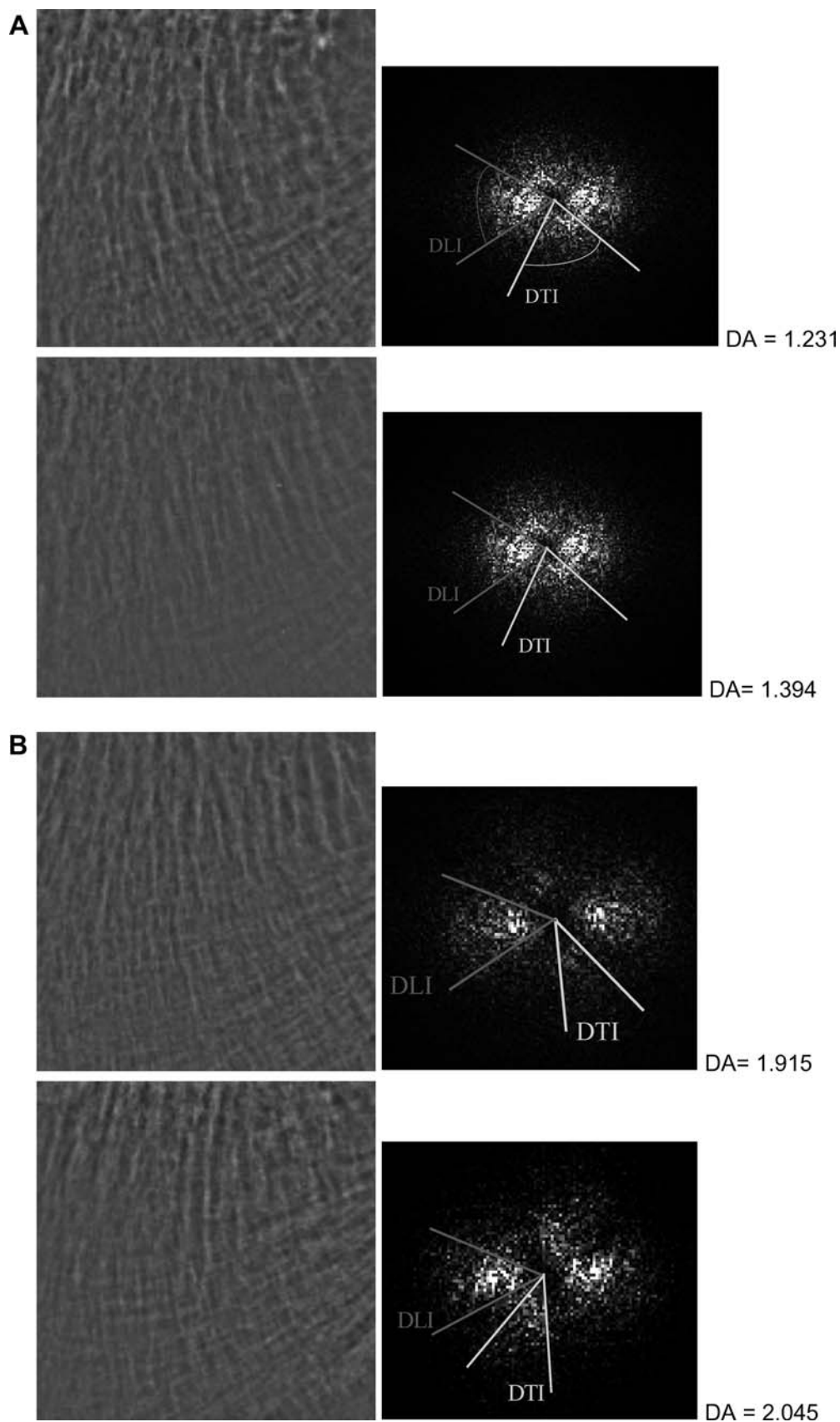
$$RMSCV = \sqrt{\frac{\sum_{j=1}^n CV_j^2}{n}} \quad (4)$$

where CV_j is the individual coefficient of variation for the subject j and n the number of subjects.

Fractal analysis

The fractal analysis was based on the fractional Brownian motion (fBm); for calculations we used the increments of fBm called fractional Gaussian noise (fGn). The maximum likelihood estimator was applied to the fGn to estimate the Hurst exponent (H). The

Fig. 4 A typical FFT spectrum of the filtered image with a cross-like shape. The FFT spectrum in this analysis is considered as an image of the magnitude repartition, and the measurements were manually performed directly on this image. *Vertical component* represents transverse trabeculae fabric and *longitudinal component* represents longitudinal trabeculae fabric. **A** represents normal subjects and **B** patients with fracture. $DA = 1.231$, $DA = 1.394$. **A** $DA = 1.915$, $DA = 2.045$. **B** *DLI* spreading angle of the longitudinal trabeculae, *DTI* spreading angle of the transverse trabeculae



higher is H, the smaller the roughness of the texture. H was estimated on each parallel line and averaged in one direction. This estimation was repeated for 36 directions (every 10°), and Hmean of the image was calculated by averaging the 36 obtained values [21].

Statistical analysis

For texture parameters, a Mann-Whitney test was used to discriminate vertebral fracture cases from the control cases. The discriminated quality of trabecular micro-architecture parameters and BMD was assessed by means of receiver-operating characteristic (ROC) curves with estimation of the associated area under the curves. Each parameter was then standardized (where the variances used for standardization were the weighted means of intra-group variances), and associations between these parameters and vertebral fracture were then assessed in the framework of logistic regression. A multivariate model was then assessed where age and FN-BMD were forced to stay in the model because of the clinical relevance of these latter variables. Analyses were realized using the SAS software (SAS institute Inc, Cary, N.C.). We have divided these two populations of vertebral fracture cases and control cases according to tertiles of FN-BMD, Hmean and DA of each two population. The distribution of vertebral fracture cases and control cases was represented for combinations of FN-BMD, Hmean and DA.

Results

Clinical data, femoral neck and lumbar spine BMD of patients with vertebral fracture and controls are described in Table 1. The two trabecular micro-architecture parameters (DA and Hmean) were estimated on the three different ROIs, and the results are presented in Table 2. For any ROI, Hmean was significantly different between both groups. For small ROIs (ROIb and ROIc), there were no significant differences. ROIa provided the best results with highly significant differences (for all parameters $P < 10^{-4}$). Therefore, the whole statistical study was performed on the results estimated

Table 1 Description of the populations of vertebral crush fractures and control cases submitted to the anisotropy measurement. HRT hormonal replacement therapy

	Controls (n = 70)	Cases (n = 39)	P
Mean ± SD			
Age (years)	68.3 ± 10.8	69.7 ± 12.5	NS
HRT, number (%)	15 (21.4)	4 (10.3)	NS
Weight (kg)	62.4 ± 10.9	63.7 ± 14.1	NS
Neck BMD (g/cm ²)	0.695 ± 0.117	0.639 ± 0.117	0.01
Lumbar spine BMD (g/cm ²)	0.918 ± 0.156	0.825 ± 0.160	0.004

Table 2 Comparisons of texture parameters between controls and osteoporosis cases in the three different regions of interest of the calcaneus. DA degree of anisotropy, Hmean fractal parameter

	Controls (n = 70) Mean ± SD	Cases (n = 39) Mean ± SD	Statistical significance P value
ROIa			
DA	1.548 ± 0.136	1.746 ± 0.169	< 10 ⁻⁴
Hmean	0.707 ± 0.031	0.662 ± 0.073	< 10 ⁻⁴
ROIb			
DA	1.527 ± 0.255	1.541 ± 0.305	0.9194
Hmean	0.702 ± 0.024	0.666 ± 0.073	0.0159
ROIc			
DA	1.686 ± 0.322	1.711 ± 0.300	0.4633
Hmean	0.664 ± 0.034	0.631 ± 0.075	0.0095

on the ROIa. In this ROI, the result of the long-term reproducibility is 2.8% for DA, and we have reanalyzed Hmean and DA according to hormonal replacement therapy status. The results are described in Table 3. Concerning only women without HRT, the Hmean and DA results of 55 control women (out of 70) and 35 fracture case patients (out of 39) remained respectively significantly different ($P = 0.004$; $P < 10^{-4}$), whereas only lumbar spine BMD was slightly lower in fracture cases ($P = 0.03$). The process was performed on ROIa by a second observer, and this second process gave a DA of 1.526 ± 0.123 in the 70 controls and 1.668 ± 0.141 in the 39 fracture cases ($P < 10^{-4}$). The same comparison restricted to the women without HRT gave a DA of 1.523 ± 0.130 in the 55 in the control groups and a DA of 1.685 ± 0.135 in the 35 fracture cases ($P < 10^{-4}$).

The ROC curves of DA and Hmean calculated for the whole population are shown in Fig. 5. The areas under curves (AUC) were estimated for these parameters and for LS and FN-BMD. The most discriminant parameters were DA and Hmean (with respectively AUCs of 0.765 and 0.683), while AUCs associated with LS-BMD and FN-BMD were lower (respectively 0.614 and 0.591).

Considering a variation of 1 SD, crude odds ratios for DA, Hmean, LS-BMD and FN-BMD calculated for the whole population are depicted in Table 4. All odds ratios were statistically significant. The odds ratios associated to Hmean and anisotropy indices were higher than the odds ratios of BMD measurements.

The odds ratios derived from a multivariate analysis are depicted in Table 5. The remaining significant odds ratios were DA and Hmean, with the highest one for DA. Age and FN-BMD were forced to stay in the model because of their clinical relevance, but the age influence was very unlikely in this model since the groups of osteoporotic fractures and of controls were age-matched.

The distribution of fracture cases and control cases in percentage according to tertiles of FN-BMD, Hmean and DA are illustrated in Fig. 6. In Fig. 6A, for the vertebral fractures cases, the highest percentage (28.2%)

Table 3 Results of Hmean and DA according to their hormonal replacement therapy status in vertebral fracture cases and control cases

	Control groups		Cases	
	Without HRT (n = 55)	With HRT (n = 15)	Without HRT (n = 35)	With HRT (n = 4)
Age (years)	70.3 ± 10.3 ^{nsB}	60.7 ± 9.1	70.5 ± 12.6	62.5 ± 10.7
Weight (kg)	62.4 ± 10.3 ^{nsNS}	62.4 ± 12.3	63.0 ± 14.4	69.2 ± 9.6
Neck BMD (g/cm ²)	0.684 ± 0.12 ^{nsNS}	0.734 ± 0.1	0.642 ± 0.12	0.619 ± 0.04
Lumbar spine BMD (g/cm ²)	0.905 ± 0.154 ^{aNS}	0.967 ± 0.158	0.825 ± 0.17	0.824 ± 0.08
Hmean	0.702 ± 0.03 ^{bA}	0.726 ± 0.03	0.670 ± 0.07	0.588 ± 0.10
DA	1.55 ± 0.14 ^{cNS}	1.54 ± 0.11	1.761 ± 0.16	1.61 ± 0.20

Difference between subjects with and without HRT in controls groups: NS, A $P < 0.01$; B $P < 0.001$. Difference between control group without HRT and cases without HRT: ns, a $P < 0.01$; b $P < 0.001$; c $P < 10^{-4}$

was obtained for the combination of the highest DA with the lowest FN-BMD. For the control cases, the highest percentage (20.0%) was obtained for the combination of the highest FN-BMD with the lowest DA. In Fig. 6B, for the vertebral fracture cases, the highest percentage of fractures (33.3%) was obtained for the combination of the lowest Hmean with the highest DA.

For the control cases, the highest percentage (22.8%) was obtained for the combination of the highest Hmean with the lowest DA. In Fig. 6C, for the vertebral cases, the highest percentage (30.8%) was obtained for the combination of the lowest Hmean with the lowest FN-BMD. For the control cases, the highest percentage (22.8%) was obtained for the combination of the highest FN-BMD with the highest Hmean. Globally, the distribution of the control cases was more homogeneous between low and high values of FN-BMD, Hmean and DA. On the contrary, the distribution of the vertebral fracture cases was more concentrated in low values of FN-BMD and Hmean and in high values of DA.

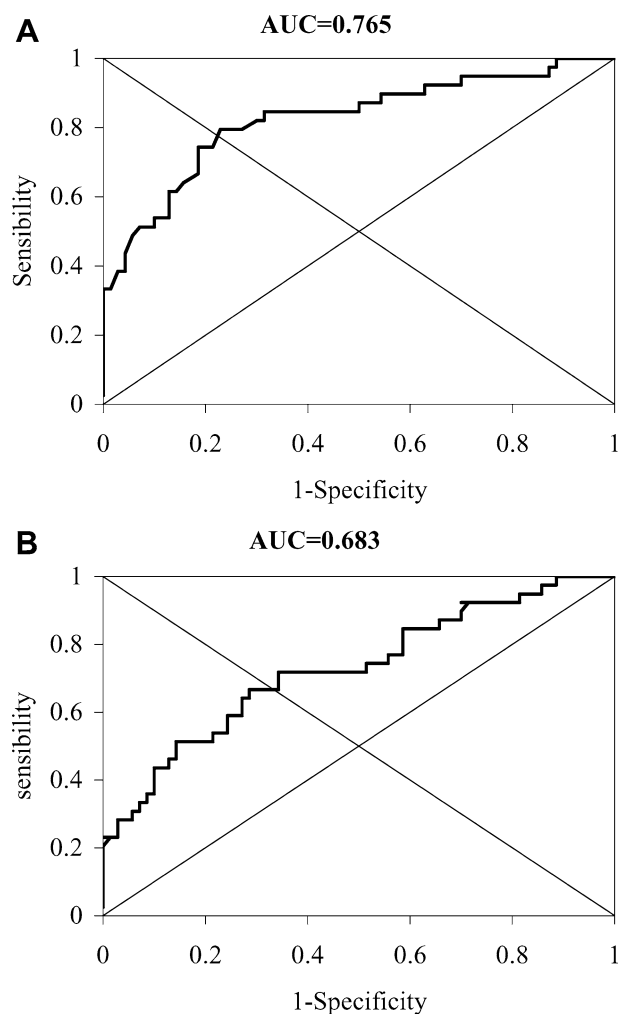


Fig. 5 Receiver operating characteristics curves for DA and Hmean. **A** DA, **B** Hmean

Discussion

These data suggest that anisotropy indicators derived from Fourier transform analysis and applied to trabecular bone radiographic images can distinguish vertebral fracture cases from control cases. Among the three ROIs of the calcaneus, the previously used 256×256-pixel ROI was more reliable than two other ROIs using 128×128-pixel areas. Several authors have previously noticed the heterogeneity of the calcaneus [27, 28]. This heterogeneity explains the importance of standardized procedure of ROI determination and could explain why ROIb and ROIc are less discriminant. The smaller size of ROIb and ROIc could constitute another explanation. Juxtacortical trabeculae could be also less sensitive to aging and osteoporosis changes. This could explain why ROIb and ROIc are less discriminant than ROIa in terms of micro-architectural parameters (Fig. 1).

Table 4 Univariate analysis expressing the odds ratios (OR) of vertebral osteoporotic fractures for the indicator of anisotropy (DA), the Hmean fractal parameter, LS and FN-BMD. CI confidence interval

	OR	95% CI	P
DA (↑ 1SD)	3.91	(2.22; 6.87)	< 0.001
Hmean (↓ 1SD)	3.08	(1.71; 5.52)	< 0.001
LS-BMD (↓ 1SD)	1.71	(1.15; 2.56)	0.009
FN-BMD (↓ 1SD)	1.56	(1.05; 2.31)	0.026

Table 5 Multivariate analysis expressing the odds ratios (*OR*) of vertebral osteoporotic fractures for the indicator of anisotropy (*DA*), the Hmean fractal parameter, age and FN-BMD. *CI* confidence interval

	OR	95% CI	<i>P</i>
DA (↑ 1SD)	6.33	(2.80; 14.30)	<0.001
H (↓ 1SD)	3.08	(1.48; 6.37)	0.002
Age (↑ 1 year)	0.97	(0.92; 1.02)	0.198
FN-BMD (↓ 1SD)	1.05	(0.99; 1.12)	0.104

For Hmean, in the present subgroup of patients with vertebral fractures, the results obtained with ROIa are similar to those obtained in a previous study [23]. We have previously shown that the fractal analysis of trabecular bone projection images was related to the 3D connectivity, the regression slope being dependent upon the degree of porosity [29]. This 2D-3D correlation has been confirmed in another study using the same fractal indicator, but another 3D analysis [30]. The 2D-3D correspondence concerning anisotropy has been investigated by Luo et al. [10]: the anisotropy evaluation derived from the MIL analysis showed a very high 2D-3D correlation, with a determination coefficient $r^2 = 0.98$. This correspondence has not been checked for our anisotropy indicators, but the results of Luo et al. [10] are of great value for interpreting our results obtained on 2D projection images. In our study, the anisotropy evaluation derived from the Fourier transform of gray levels was very reliable. From a practical point of view, it is very interesting to characterize anisotropy on this kind of easily obtained image. The first reason is that the analysis is directly carried out on the gray level images without previous binarization. For most methods, such as MIL and line fraction deviation, segmentation is necessary in order to work on binary images. The resolution obtained on *in vivo* images leads to partial volume effect, therefore segmentation of the image into bone and marrow phases may be difficult [31]. The second reason is that the FFT is the direct reflection of the structure orientation. Indeed, it is possible visually to distinguish on the FFT spectrum the global orientation of the structure. Among the parameters that we have measured in our experiments, the best results were obtained for DA whatever the statistical approach. The long-term reproducibility of this parameter is sufficient since the difference between the mean DA of vertebral fracture cases and control cases was 4.5 times the long-term reproducibility value. The DLI and DTI measurements on FFT spectrum are operator dependent and time consuming; it is the main limitation of the method, but the automatization clearly represents the future of this technique. To take into account the present limitation linked to the manual processing, we have performed a second analysis by an unskilled observer, and the statistical difference between fracture and control cases remained highly significant (see the sections Methods and Results).

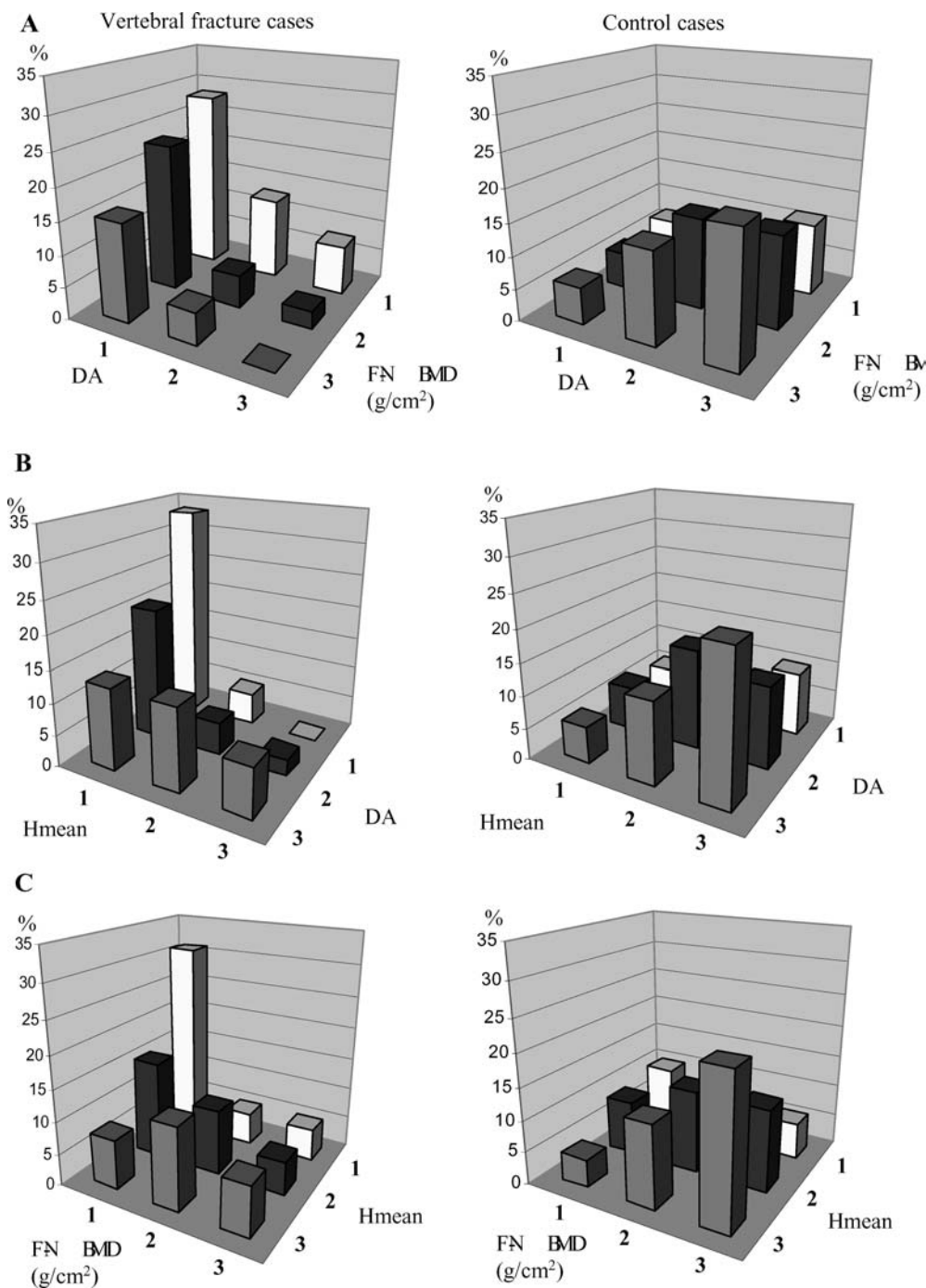
Fractal analysis was previously used to evaluate anisotropy [15, 17], but the interpretation was very difficult since fractal analysis is an index of roughness of images. The meaning of the roughness orientation remains questionable. In the present study, Hmean was used as a texture roughness indicator and not as an anisotropy indicator [21, 22, 23].

In our study, osteoporotic patients presented a higher degree of micro-architectural anisotropy on the radiographic bone images of calcaneus than controls. At the present time, there is no clear response about the question of gain or loss of anisotropy in osteoporosis. The relationship between biomechanical anisotropy and micro-architectural anisotropy changes is not totally clarified. We could think that the most resistant bones have a higher degree of micro-architectural anisotropy because they are more resistant in a preferential direction. On the other hand, we can consider that osteoporosis is characterized by a preferential loss of trabeculae having the less mechanical competence. For example, the horizontal trabeculae disappear first with age at the vertebrae, leading to a higher degree of anisotropy [32]. The Singh index evaluating the progressive preferential loss of oriented trabecular systems at the femoral neck has shown the same kind of phenomenon, leading to a higher degree of anisotropy in osteoporotic patients [33]. Our results are in accordance with those of Newitt et al. [11]. They have also found a higher DA in osteopenic patients at the radius with images obtained by magnetic resonance imaging, the anisotropy assessment being based on the MIL method [11]. Wigderowitz et al. [16] used the spectral analysis on bone radiographs at the distal radius; they observed a preferential orthogonal 2D structure in fractured patients and explained this observation by the fact that transverse trabeculae are the first to be absorbed at the radius. Zhao et al. have hypothesized a biphasic phase [34]. In the initial years, trabecular thinning would occur and the trabecular structure become more isotropic. In the later years, the remaining trabeculae would be more widely separated, less connected and some more thickened, resulting in an increase in trabecular anisotropy [34].

Jhamaria et al. [25] have found in the great tuberosity of the os calcis that the posterior tensile trabeculae are first removed in osteoporosis. Later in the evolution of the disease, the compression trabeculae from the subtalar joint are reduced in number and become thinner [25]. The DA relating to the degree of disorientation of transversal and longitudinal trabeculae was higher in osteoporotic patients; this increase could be explained by a change in the repartition of trabeculae belonging to compressive or tensile networks.

In a multivariate logistic regression analysis, DA remained despite the fact that FN-BMD was introduced into the model; similarly, DA remained when Hmean was introduced. These results suggest that anisotropy indicators and Hmean are complementary to BMD measurements for fracture risk determination. However, the absence of site-matched gold-standard BMD

Fig. 6 Distribution of vertebral fracture cases and control cases in percentage according to tertiles of FN-BMD, Hmean and DA. The following combinations of parameters are represented: FN-BMD vs. DA (A), Hmean vs. DA (B) and FN-BMD vs. Hmean (C)



measurements is a limitation. Since the BMD of the calcaneus is not performed in clinical routine, we preferred to compare only with the usual BMD measurements used for the diagnosis of osteoporosis. In relation to the high odds ratios obtained, it is probable that the additional information provided by Hmean and DA measurements is due to the new technique approach and to a lower extent to the measurement site.

In conclusion, the anisotropy indicators applied to calcaneus radiographs can provide a reliable character-

ization with a method derived from the Fourier transform of the gray levels. These data suggest that when added to BMD and fractal analysis, the anisotropy evaluation can help to improve the evaluation of OP fracture risk. Prospective studies are needed to better understand the changes of anisotropy in osteoporosis and their ability to help the fracture risk prediction.

Acknowledgements We acknowledge W. Hohley's critical discussion of the paper and English corrections.

References

1. Turner CH (2002) Biomechanics of bone: determinants of skeletal fragility and bone quality. *Bone* 13:97–104
2. Genant HK, Cooper C, Poor G et al (1999) Interim report and recommendations of the World Health Organization Task Force for Osteoporosis. *Osteoporos Int* 10:259–264
3. Odgaard A (1997) Three-dimensional methods for quantification of cancellous bone architecture. *Bone* 20:315–328
4. Mosekilde L, Viidik A, Mosekilde L (1985) Correlation between the compressive strength of iliac and vertebral trabecular bone in normal individuals. *Bone* 6:291–295
5. Geraets WGM, Van der Stelt PF, Netelenbos CJ, Elders PJM (1990) A new method for automatic recognition of the trabecular pattern. *J Bone Miner Res* 5:227–233
6. Majumdar S, Khotari M, Augat P, Newitt DC, Link TM, Lin JC, Lang T, Lu Y, Genant HK (1998) High-resolution magnetic resonance imaging: three dimensional trabecular bone architecture and biochemical properties. *Bone* 22:445–454
7. Mosekilde L (1988) Age-related changes in vertebral trabecular bone architecture assessed by a new method. *Bone* 9:247–250
8. Parfitt AM (1992) Implications of architecture for the pathogenesis and prevention of vertebral fracture. *Bone* 13:S41–S47
9. Harrigan TP, Mann RW (1984) Characterization of microstructural anisotropy in orthotropic materials using a second rank tensor. *J Mater Sci* 19:761–767
10. Luo G, Kinney JH, Kaufman JJ, Haupt D, Chiabrera A, Siffert RS (1999) Relationship between plain radiographic patterns and three-dimensional trabecular architecture in the human calcaneus. *Osteoporos Int* 9:339–345
11. Newitt DC, Majumdar S, Van Rietbergen B, Ingersleben GV, Harris ST, Genant HK, Chesnut C, Garnero P, Mac Donald B (2002) In vivo assessment of architecture and micro-finite element analysis derived indices of mechanical properties of trabecular bone in the radius. *Osteoporos Int* 13:6–17
12. Odgaard A, Jensen EB, Gundersen HJ (1990) Estimation of structural anisotropy based on volume orientation. A new concept. *J Microscop* 157:149–162
13. Cruz-Orive LM, Karlsson LM, Larsen SE, Wainschein F (1992) Characterizing anisotropy: a new concept. *Micron Microsc Acta* 23:75–76
14. Geraets WGM, Van der Stelt PF, Lips P, Elders PJM, van Ginkel FC, Burger EH (1997) Orientation of the trabecular pattern of the distal radius around the menopause. *J Biomech* 30:363–70
15. Lespessailles E, Jacquet G, Harba R, Jennane R, Loussot T, Viala JF, Benhamou CL (1996) Anisotropy measurement obtained by fractal analysis of trabecular bone at the calcaneus and radius. *Rev Rhum* 63:337–343
16. Wigderowitz CA, Abel EW, Rowley DI (1997) Evaluation of cancellous structure in the distal radius using spectral analysis. *Clin Orthop* 335:152–161
17. Jiang C, Pitt RE, Bertram JEA, Aneshansley DJ (1999) Fractal-based image texture analysis of trabecular bone architecture. *Med Biol Eng Comput* 37:413–418
18. Caligiuri P, Giger ML, Favus MJ, Jia H, Doi K, Dixon LB (1993) Computerized radiographic analysis of osteoporosis: preliminary evaluation. *Radiology* 186:471–474
19. Caldwell CB, Willett K, Cuncins AV, Hearn TC (1995) Characterization of vertebral strength using digital radiographic analysis of bone structure. *Med Phys* 22:611–615
20. Geraets WGM (1998) Comparison of two methods for measuring orientation. *Bone* 23:383–388
21. Benhamou CL, Lespessailles E, Jacquet G, Harba R, Jennane R, Loussot T, Tourliere D, Ohley W (1994) Fractal organization of trabecular bone images on calcaneus radiographs. *J Bone Miner Res* 9:1909–1918
22. Pothuau L, Lespessailles E, Harba R, Jennane R, Royant V, Eynard E, Benhamou CL (1998) Fractal analysis of trabecular bone texture on radiographs: discriminant value in postmenopausal osteoporosis. *Osteoporos Int* 8:618–625
23. Benhamou CL, Poupon S, Lespessailles E, Loiseau S, Jennane R, Siroux V, Ohley W, Pothuau L (2001) Fractal analysis of radiographic trabecular bone texture and bone mineral density: two complementary parameters related to osteoporotic fractures. *J Bone Miner Res* 16:697–704
24. Genant HK, Wu CY, van Kuijk C, Newitt MC (1993) Vertebral fracture assessment using semiquantitative technique. *J Bone Miner Res* 8:1137–1148
25. Jhamaria NL, Lal KB, Udawat M, Banerji P, Kabra SG (1983) The trabecular pattern of the calcaneus as an index of osteoporosis. *J Bone Joint Surg* 65:195–198
26. Glüer C, Blake G, Lu Y, Blunt BA, Jergas M, Genant HK (1995) Accurate assessment of precision errors: how to measure the reproducibility of bone densitometry techniques. *Osteoporos Int* 5:262–270
27. Lin JC, Amling M, Newitt DC, Selby K, Srivastav SK, Delling G, Genant HK and Majumdar S (1998) Heterogeneity of trabecular bone structure in the calcaneus using magnetic resonance imaging. *Osteoporos Int* 8:16–24
28. Chappard C, Laugier P, Fournier B, Roux C, Berger G (1997) Assessment of the relationship between broadband ultrasound attenuation and bone mineral density at the calcaneus using BUA imaging and DXA. *Osteoporos Int* 7:316–322
29. Pothuau L, Benhamou CL, Porion P, Lespessailles E, Harba R, Levitz P (2000) Fractal dimension of trabecular bone projection texture is related to three-dimensional microarchitecture. *J Bone Miner Res* 15:691–699
30. Jennane R, Ohley WJ, Majumdar S, Lemineur G (2001) Fractal analysis of bone X-ray tomographic microscopy projections. *IEEE Trans Med Imag* 20:443–449
31. Majumdar S, Genant HK, Grampp S, Newitt DC, Truong VH, Lin JC, Mathur A (1997) Correlation of trabecular bone structure with age, bone mineral density, and osteoporotic status: in vivo studies in the distal radius using high resolution magnetic resonance imaging. *J Bone Min Res* 12:111–118
32. Mosekilde L (1989) Sex differences in age related loss of vertebral trabecular bone mass and structure biomechanical consequences. *Bone* 10:425–432
33. Singh M, Nagrath AR, Maini PS (1970) Changes in trabecular pattern of the upper end of the femur as an index of osteoporosis. *J Bone Joint Surg* 52A:457–467
34. Zhao J, Jiang Y, Recker RR, Draper MW, Genant HK (2001) Iliac three-dimensional trabecular microarchitecture in premenopausal healthy women and postmenopausal osteoporotic women with and without fracture. *J Bone Miner Res* 17:S468